ORIGINAL RESEARCH ARTICLE

Charge Transport Mechanism in a PECVD Deposited Low-*k* SiOCH Dielectric

T. V. Perevalov[1] · A. A. Gismatulin[1] · V. A. Gritsenko[1,2] · H. Xu[3,4] · J. Zhang[4] · K. A. Vorotilov[5] · M. R. Baklanov[4,5]

Abstract

One of the most important issues during the selection of low-*k* dielectrics is related to their intrinsic properties including their electric breakdown and leakage current that are predominantly determined by conduction mechanisms. This study is devoted to elucidating the charge transport mechanism in the SiOCH low-*k* dielectric films fabricated by plasma-enhanced chemical vapor deposition. By analyzing four bulk-limited models of the charge transport it was found that only the Nasyrov–Gritsenko model of phonon-assisted electron tunneling between neutral traps describes the experimental *I–V–T* characteristics with all the fitting parameters with reasonable physical values. The obtained thermal trap energy value 1.2 eV is confirmed independently by photoluminescence spectroscopy data analysis. The trap nature and comparison of the obtained results with the corresponding data for low-*k* films with similar chemical composition and deposited by the spin-on-glass technology using self-assembling chemistry is discussed. It is hypothesized that the defect with ionization energy of 1.2 eV is the oxygen divacancy.

Introduction

Low dielectric constant (low-*k*) materials play an important role in ultra-large-scale integration (ULSI) interconnects to overcome the problems of signal delay and power consumption associated with a reduced metal pitch and thickness.[1] The low-*k* materials presently selected by industry for Cu damascene integration technology are mainly carbon-doped oxides (also termed as organosilica glasses, OSG) fabricated by plasma-enhanced chemical vapor deposition (PECVD).[2] They may have k-values in the range from 3.0 to 2.0, depending on porosity, which is generated using sacrificial porogens. Recently, some new conductors such as Ru, Mo, and W have been explored because of their low resistivity in narrow lines and better resistance to electromigration in comparison with Cu. These conductors can be patterned by using plasma etch technology and, therefore, they are suitable for subtractive integration (metal etch first) allowing a significant reduction of the plasma damage and the improvement of compatibility with thin diffusion barriers.[3,4] Subtractive integration needs the deposition of flowable low-*k* dielectrics that can be fabricated by using spin-on-glass (SOG) technology.[5] SOG low-*k* materials are considered promising for subtractive integration due to their improved mechanical properties and excellent gap filling capability.

Both PECVD and SOG dielectrics have similar matrix structures and chemical compositions. However, the porogen molecules used in PECVD are co-deposited together with the matrix precursors and originally randomly distributed inside the matrix and can leave an amorphous carbon-like residue (porogen residue) after the UV-assisted thermal curing. The porogen residues in PECVD low-*k* materials can act as charge traps and can be responsible for the leakage current and time-dependent dielectric breakdown (TDDB).[6–8] The properties of trap states can determine the reliability of

✉ T. V. Perevalov
    timson@isp.nsc.ru

1   Rzhanov Institute of Semiconductor Physics SB RAS, 13 Lavrentiev Ave., Novosibirsk, Russia 630090

2   Novosibirsk State Technical University, 20 Marks Ave., Novosibirsk, Russia 630073

3   China United Network Communications Co., Ltd., 9 Iuomashi St, Xicheng District, Beijing 100052, China

4   North China University of Technology, 5 Jinyuanzhuang Rd., Shijingshan District, Beijing 100144, China

5   MIREA, Russian Technological University, 78 Vernadsky Ave., Moscow, Russia 119454

integrated low-*k* materials and it is one of the central problems for ULSI devices. In particular, the trapped charge may change the barrier height and provide a low-energy conduction pathway.[9] The intermetal dielectric (IMD) leakage-current during the TDDB testing usually decreases at the initial time and it is typically identified as the "trapping phase" at the defects within the low-*k* charges and inhibits the leakage. Simultaneously, new defects are generated due to high stress conditions, so the leakage then begins to increase as the "detrapping", or the defect generation phase starts to dominate.

The SOG deposited films based on self-assembling chemistry are normally porogen residue free.[8] For these materials, the important trap contribution was also identified in the leakage current.[10–12] It was shown that these traps are related to excess silicon (Si-Si or Si-Si-Si defects) in low-*k* films and the charge transport occurs via the phonon-assisted electron tunnelling between neutral traps.

The charge transport mechanism in low-*k* is still not fully understood although it has been extensively studied in the past. The most important features of these observations were discussed and summarized in the review papers by Ogawa[1] and Wu.[13] In short, the charge transfer mechanism in low-k materials depends on their composition and manufacturing procedure and can change from one dominant regime to another. It has been shown that at very high bias (~5 to 6 MV/cm), the leakage current in integrated low-k dielectrics follows Fowler–Nordheim (FN) tunneling. At a lower bias, the dominant transport mechanism appears to be Schottky emission (SE) or Poole–Frenkel (PF) conductivity. Many researchers believe that the pore wall is a dominant pass for the leakage. This opinion is partly based on theoretical calculations by Kayaba and Kikkawa, who showed that the magnitude of electrical fields in porous low-k dielectrics has a maximum field strength at the air/skeleton interfaces.[14] It is also known that the leakage current is highly dependent on concentration of adsorbed moisture if the pore wall contains hydrophilic adsorption sites such as Si-H and Si-OH formed due to unoptimized curing or processing damage.[1] It has also been shown that the leakage current depends on the presence of amorphous carbon-like porogen residue formed from the destructed porogen during too aggressive UV curing. In this case, the leakage current increases with porosity, since the higher porosity requires more porogen.[15,16] Although direct evidence is difficult to find, it was intuitively assumed that both adsorbed moisture and porogen residues are mainly located on the pore walls. Meanwhile, the accurate evaluation of the leakage current using low-k dielectrics with precisely controlled composition showed no dependence on porosity.[17] Materials with different porosity have different pore surface area and therefore the absence of this dependence suggests that the pore surface did not play a key role. However, an increase in porosity leads to lower breakdown fields, which is explained by the large amount of

cage structures (suboxides) in the film. The same conclusion was made by Wu.[13] The presence of a suboxide is associated with oxygen deficiency-related defects[18] and, therefore, has an important contribution to the leakage current if the dominant influence of adsorbed moisture and porogen residue is excluded. All these observations suggest that the leakage current mechanisms are not entirely clear[1,19] and, probably, are very sensitive to chemical composition and technological procedures used for their integration.

Most previous studies are limited in the used charge transport models.[20] So, what do inconsistent data predict? Namely, these are the space-charge-limited current model with trap ionization energy $W = 0.17$ eV at a low electric field and Frenkel model with $W \approx 2$ eV at a high electric field.[20] The models involving the electron-phonon interaction are not considered.

Thus, in this work, we aimed at reliably establishing the charge transport mechanism and determining the trap energy parameter values in the standard PECVD SiOCH low-*k* dielectric, which is currently used in the ULSI technology with Cu-based damascene technology. Understanding the charge transport mechanism is a crucial step towards understanding the nature of the traps responsible for leakage current and electric breakdown. In addition, it allows to carry out a comparative analysis of the conduction properties of PECVD and SOG films, which is useful for the selection of low-*k* materials for future technology nodes.

Materials and Methods

The SiCOH low-*k* materials were obtained from industrial sources as blank films. The films were deposited on 300-mm phosphorus-doped Si(1 0 0) wafers with resistivity 7.5 ohm · cm by PECVD using diethoxymethylsilane (DEMS) as a network matrix precursor and alpha-terpinene (ATRP) as a precursor of sacrificial porogen.[21] Both molecules (matrix and porogen precursors) were simultaneously introduced into the plasma chamber and formed a "hybrid" film consisting of an organosilica matrix with organic inclusions. The organic phase (porogen) is removed by the post-deposition treatment, which is based on ultraviolet (UV)-assisted thermal curing. A broadband UV source with a wavelength >200 nm was used for the curing. After the complete curing at T ≈ 400°C, the film became porous and had ultra-low-*k* properties (porosity ≈ 24% and $k \approx 2.5$). Optical characteristics and chemical composition of these films were evaluated by using ellipsometry, XPS, FTIR and Raman spectroscopy, and the results are reported in our previous paper.[22] The chemical composition of these films was quite typical for PECVD SiOCH films. One feature important for our present analysis

is the presence of s–p^3 and s–p^2 hybridized C-C bonds that can be attributed to the presence of porogen residue.

The photoluminescence (PL) and photoluminescence excitation (PLE) spectra were measured on Jasco FP-8300 with a Xe lamp as a light source. The excitation and emission spectra were recorded in the quantum energy range from 1.77 eV to 5.4 eV. The electron energy loss spectra (EELS) were obtained by using the Riber LAS-2000 spectrometer. The incident electron beam was energy 200 eV. The amplitude of the modulation signal for the synchronous detector was 0.3 V.

For the charge transport measurements, the magnesium contact with the area of 5×10^{-3} cm^2 was deposited on top of the annealed PECVD low-*k* dielectric. To stabilize the low-*k* dielectric and remove the adsorbed impurities, the samples were annealed at 300°C in Ar atmosphere for 30 min just before deposition of metal electrodes. The continuous aluminum contact was deposited on the back side of silicon substrate. The current-voltage characteristics at different temperature (*I–V–T*) measurements were carried out on a Keithley 2400 device at a positive potential on magnesium; the lower contact was grounded. Sensitivity of the current measuring device is 10 pA. The device has a current limit of 10 μA during measurement. *I–V–T* measurements were carried out from 0 MV/cm to 4.5 MV/cm at a voltage rate of 0.9 V/s. The low-*k* film thickness was 220 nm. Thus, the bulk-limited charge transport models like that of Frenkel,[23,24] Hill–Adachi (H–A),[25,26] Makram-Ebeid and Lannoo (ME-L),[27] and Nasyrov–Gritsenko (N–G)[28] were used to describe *I–V–T* characteristics. The Frenkel model describes the charge transport through isolated Coulomb traps by the current density expression (Fig. 1a):

$$j = eN^{2/3} \nu \exp\left(-\frac{W - \left(\frac{e^3}{\pi \varepsilon_\infty \varepsilon_0}\right)^{1/2} \sqrt{F}}{kT} \right), \quad (1)$$

The Hill–Adachi model of overlapping Coulomb potentials considers the effect of neighboring traps at their high concentration (Fig. 1b).

$$j = eN^{2/3} 2\nu \exp\left(-\frac{W - \frac{e^2}{\pi \varepsilon_\infty \varepsilon_0 s}}{kT} \right) \sinh\left(\frac{eFs}{2kT}\right) \quad (2)$$

The Makram-Ebeid and Lannoo model describes the neutral trap multiphonon ionization mechanism. After the phonon energy absorption, an electron leaves a trap and tunnels into the conduction band, where it moves across the electric field until it is captured by the neighboring trap or the reaches the contact. The current density in the ME–L model has the form (Fig. 1c)[27]
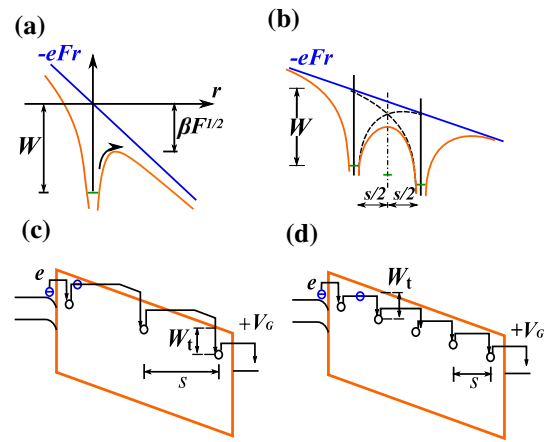

Fig. 1 Energy diagrams illustrating the various charge transport model mechanisms: Frenkel (a); Hill–Adachi (b); Makram-Ebeid and Lannoo (c); Nasyrov–Gritsenko (d).

$$j = eN^{2/3} \sum \exp\left(\frac{nW_{ph}}{2kT} - \frac{W_{opt} - W_t}{W_{ph}} \coth \frac{W_{ph}}{2kT} \right)$$
$$\times I_n\left(\frac{W_{opt} - W_t}{W_{ph} \sinh\left(W_{ph}/2kT\right)} \right) P_i\left(W_t + nW_{ph}\right) \quad (3)$$
$$P_i = \frac{eF}{2\sqrt{2m^* W}} \exp\left(-\frac{4}{3} \frac{\sqrt{2m^*}}{\hbar e F} W^{3/2} \right)$$

The N–G model of phonon-assisted electron tunneling between neutral neighboring traps describes the charge transport at a high trap concentration. With a small distance between neighboring traps, after ionization, it is more beneficial for the electron to tunnel to the neighboring trap without entering the conduction band. The current density in that case is described by the formula (Fig. 1d):

$$j = eN^{\frac{2}{3}} \frac{2\sqrt{\pi}\hbar W_t}{m^* s^2 \sqrt{2kT\left(W_{opt} - W_t\right)}} \exp\left(-\frac{W_{opt} - W_t}{kT} \right)$$
$$\times \exp\left(-\frac{2s\sqrt{2m^* W_t}}{\hbar} \right) \sinh\left(\frac{eFs}{2kT} \right) \quad (4)$$

In Eqs. 1–4, $N = s^{-3}$ is the trap concentration, s is the average distance between traps, $\nu = W/h$ is the attempt-to-escape factor, W is the trap ionization energy, e is the electron charge, F is the electric field, $\varepsilon_\infty = n^2$ is the high-frequency dielectric permittivity, n is the refractive index, ε_0 is the dielectric constant, k is the Boltzmann constant, T is the temperature, W_t is the thermal trap energy, W_{opt} is the optical trap energy, W_{ph} is the phonon energy, I_n is the modified Bessel function, P_i is the tunneling probability through a triangular barrier, m^* is the electron effective mass, $\hbar$ is the Plank's constant.

Results and Discussion

The experimental and theoretical *I–V–T* characteristics, obtained by using four charge transport models, are presented in Fig. 2. The *I–V–T* characteristics were measured in the range of 0–4.5 MV/cm. However, the current from 0 MV/cm to 3.5 MV/cm is a sum of the noise and displacement currents. The current near the 3.5 MV/cm is at the limit of the device sensitivity threshold (10 pA). The displacement current does not contain information about the charge transport in the dielectric and, therefore, has not been studied specifically. The current from 3.5 MV/cm to 4.5 MV/cm was enough for the simulation within the bulk-limited models, since the best agreement between the experiment and theory for these models is achieved in strong fields. The studied films show the breakdown at a field of about 5 MV/cm. However, it is necessary to note that this value is lower than the breakdown field requested for OSG low-k films selected for industrial application (>7 MV). The breakdown field is very dependent of the samples preparation and the test structures used for this purpose. Normally, the specialized test structures known as planar capacitors are used for this purpose.[29] Therefore, the measured value of 5 MV mostly reflects our test structure compared to the intrinsic property of the studied low-k film. However, the study of breakdown field was not the primary goal of our research

One can see that the experimental data can be formally described by any model with appropriate fitting parameters. The Frenkel effect model gives the trap ionization energy value $W = 0.9$ eV. Thus, the attempt-to-escape factor[24] is $\nu \approx W/h = 2.2 \times 10^{14}$ s^{-1}. But the Frenkel model exhibits the anomalously low trap concentration value of $N = 50$ cm^{-3} and the high-frequency dielectric constant value $\varepsilon_\infty = 6$ is too high for low-k dielectrics. Therefore, the Frenkel model is not suitable for describing the charge transport mechanism in the studied PECVD low-k SiOCH dielectric.

H–A model describe the *I-V-T* characteristics by using the reasonable trap concentration $N = 5.6 \times 10^{20}$ cm^{-3} and high-frequency dielectric constant $\varepsilon_\infty = 1.55$ values. But to simulate the experimental data, we require a suspiciously high trap energy value $W = 3.1$ eV and an unphysically low attempt-to-escape factor value $\nu = 2.5 \times 10^2$ s^{-1}. The estimation of $\nu = W/h$ predicts a value of about 10^{14} s^{-1} by the order of magnitude. So, the charge transport for the studied PECVD low-k SiOCH dielectrics is not carried out by the H–A model.

The simulation within the ME–L model simulation gives a quite reasonable value of thermal trap energy $W_t = 0.95$ eV, optical trap energy $W_{opt} = 2.9$ eV and effective mass $m^* = 1$ m_e. However, it predicts a very low trap concentration value $N = 10^{11}$ cm^{-3}. The ME–L model is applicable at $N = 10^{18}$-10^{19} cm^{-3}. One can conclude that the ME–L model does not describe the charge transport in the PECVD low-k SiOCH structure.

Only the Nasyrov–Gritsenko model describes the experimental *I–V–T* characteristics consistently, that is, all the fitting parameters of the model have reasonable physical values: thermal trap energy $W_t = 1.2$ eV, optical trap energy $W_{opt} = 2.4$ eV, trap concentration $N = 3.0 \times 10^{20}$ cm^{-3}, effective mass $m^* = 2.7 m_e$. The overestimated effective mass value is explained by the fact that the used model assumed a uniform electric field ($F = $ const). To account for the spatial charge distribution, the Poisson equation and

Fig. 2 Experimental current-voltage characteristics at different temperatures (characters) and the theoretical ones (dashed lines) simulated within (a) Frenkel, (b) Hill–Adachi, (c) Makram-Ebeid and Lannoo, (d) Nasyrov–Gritsenko models. Model parameters are included in the figures.
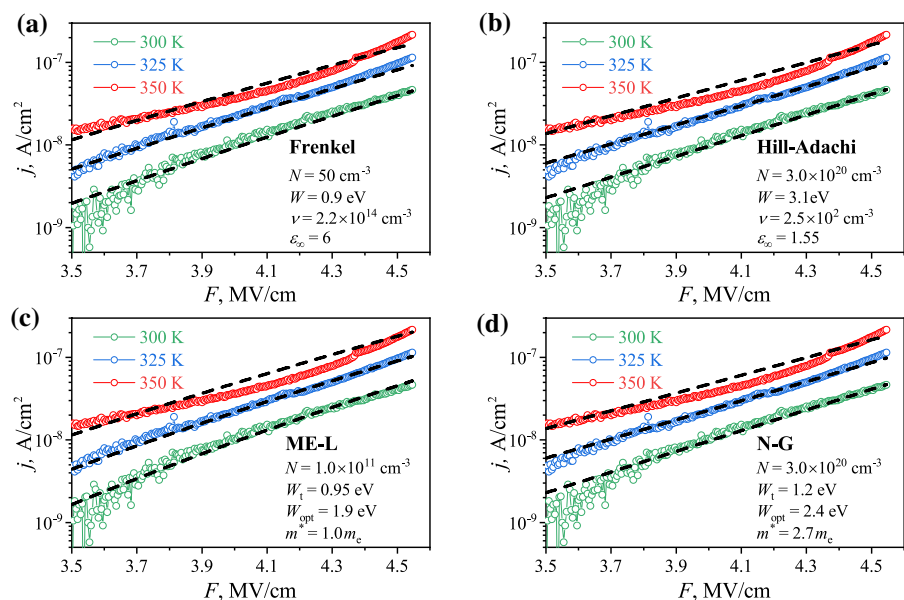
Shockley-Read-Hall statistics for trap occupation should be integrated into the N–G equation.[30] This is quite a constructive hypothesis, given the high trap concentration, but its proof significantly complicates the model. Thus, we conclude that the charge transport in the PECVD SiOCH low-*k* dielectric is carried out by the Nasyrov–Gritsenko mechanism of phonon-assisted electron tunneling between the neutral traps.

To check the obtained trap parameter values predicted from the charge transport simulation, we estimated the trap ionization energy from the measured photoluminescence (PL) and photoluminescence excitation (PLE) spectra. The idea of this estimation is based on the rule of thumb, according to which half of the Stokes shift of luminescence in a dielectric coincides with the thermal trap energy. This rule holds for such dielectrics as Si_3N_4, Al_2O_3, HfO_2, ZrO_2 and Ta_2O_5.[31–35]

The PL spectrum of the studied film exhibits the most intense peak at 2.25 eV (Fig. 3). Emission intensity depends on the excitation light energy, and the maximum emission is observed at an excitation 4.2–4.6 eV (Fig. 4). Thus, the thermal trap energy value for the studied PECVD low-*k* dielectric evaluated from the PL Stokes shift is in the range of 1.1–1.2 eV. These values are remarkably consistent with $W_t = 1.2$ eV obtained from the analysis of *I–V–T* characteristics within the N-G model. Thus, luminescent spectroscopy, independently, indirectly confirms the correctness of the simulation results for the *I–V–T* characteristics and our conclusion that the charge transport is carried out by the N–G mechanism.

The second derivative of the inelastic scattered electrons (EELS) for the studied low-k dielectric shows a significant wide peak with maxima in range of 6.1–6.8 eV (Fig. 5). The peak at 6.8 eV could be referred to the triple silicon cluster Si–Si–Si (or oxygen divacancy) as in SiO_2.[36,37] It is acceptable to assume that the maximum at 6.1 eV is also caused by oxygen vacancies in silicon oxide clusters, namely, the E' center (vacancy with a trapped hole) on the surface.[36] The observed peak at the energy range of 4.1 eV is explained by the electronic transitions onto other defect types, probably
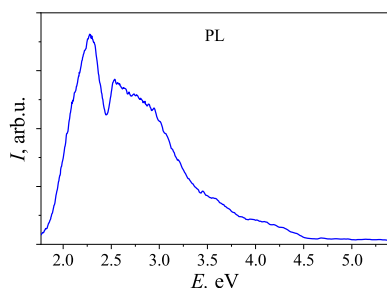
silicon vacancies or their combination with the organics.[38] Thus, EELS spectroscopy data confirm the presence of defects in the studied low-κ dielectric film associated with excess silicon, namely, oxygen divacancies.

Unfortunately, the obtained results do not allow us to reveal the nature of the traps which are responsible for the charge transport in the studied films. On the one hand, $W_t = 1.2$ eV was previously obtained for SOG-deposited methyl-terminated low-*k* dielectrics where it was definitely related to the Si–Si–Si bond (oxygen divacancy).[11] This conclusion was based on the density functional simulation, luminescent spectroscopy and a comparison with the known data for silicon oxide. In addition, the PL maximum at 2.25 eV could be caused by silicon clusters in the film as it was interpreted previously for silicon dioxide.[39] On the other hand, for the studied film, the positions of maxima in PL and PLE spectra differ from those for methyl-terminated SOG films and silicon oxide.[11] The reason for the difference is related to the presence of carbon (porogen) residue that was detected by Raman spectroscopy. The observed PL bands at 2.2 eV are similar to those observed in carbon-incorporated porous silicon oxide.[40] Then the assumption that $W_t = 1.2$ eV in the studied PECVD low-*k* dielectric film due to the Si–Si–Si defect might be questionable.

Strictly speaking, there is no reason to exclude oxygen vacancies (divacancies) from the list of defects that play a key role in the PECVD low-*k* SiOCH film conductivity.
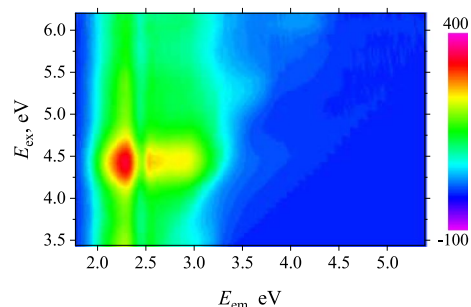

Fig. 4 A map of PL intensity depending on the PL excitation energy (PLE spectrum) for the PECVD low-*k* SiOCH film.

Fig. 3 PL spectrum measured at the excitation by quantum energy 5.4 eV for the PECVD low-*k* SiOCH film.
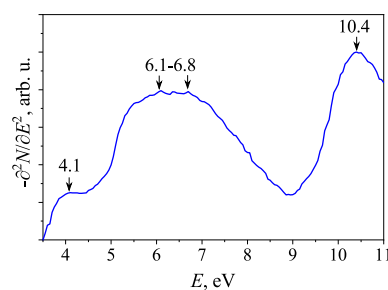

Fig. 5 EELS of the studied low-k dielectric film.

Indirect data indicating an increase in the film conductivity after UV irradiation to remove the porogen residue can be interpreted both and as an increase in the carbon residues (sp^2 carbon) concentration due to the porogen dissociation, as an increase in the concentration of oxygen vacancies due to the rupture of Si-CH$_x$ bonds with leaving Si dangling bonds that can form Si–Si or Si–Si–Si defects after a short-range structural rearrangement. Similarly, the decrease in the conductivity of low-k films due to their thermal annealing can be explained both by the porogen residue removal without its decomposition and by the fact that Si–CH$_x$ bonds do not break in this process and the oxygen vacancies formation probability decreases. Thus, in the present article, we propose an alternative interpretation of the defect nature responsible for the conductivity and breakdown of PECVD low-k dielectrics: such defects can be Si–Si and Si–S–Si (vacancies and oxygen divacancy). This alternative is supported by the results of the I–V–T characteristics analysis and the comparison with the methyl-terminated OSG low-k dielectrics. In addition, oxygen vacancies are key defects determining electrophysical properties in a wide spectrum of oxide dielectric.

Conclusions

In conclusion, the charge transport mechanism of PECVD low-k SiOCH dielectrics was investigated. The I–V–T characteristics of the studied dielectric films were analyzed using the four bulk-limited models including those involving the phonon-assisted mechanism of charge transport. It was found that the Frenkel model of thermal ionization of an isolated Coulomb trap in an electric field, the Hill–Adachi model of overlapping Coulomb traps and the Makram-Ebeid and Lannoo model of isolated trap ionization describe the charge transport only when unphysical fitting parameters are used. Only the Nasyrov–Gritsenko model of phonon-assisted electron tunneling between neutral traps gives a good agreement with the experiment with acceptable parameters: thermal trap energy $W_t = 1.2$ eV, optical energy $W_{opt} = 2.4$ eV, effective mass $m^* = 2.7\ m_e$ and trap concentration $N = 3.0 \times 10^{20}$ cm^{-3}. The estimation of the thermal trap energy as half of the Stokes shift of photoluminescence for the studied film gives a value close to that obtained from the simulation using the Nasyrov–Gritsenko model. Thus, it is concluded that the charge transport in a PECVD low-k SiOCH dielectric is described by the phonon-assisted electron tunneling between neutral traps similar to SOG materials reported in our previous work although data obtained by Raman spectroscopy[19] and PL/PLE data show porogen residue in the studied PECVD films, which also influences their conductivity mechanisms. At the same time the PL spectroscopy data, as well as electron energy loss spectrum features, are also interpreted as a signal from oxygen-deficient defects types as in silicon oxide. The trap nature responsible for the studied film conductivity and breakdown is discussed. A reasonable and novel assumption that such a defect could be interpreted both as carbon residues after the porogen dissociation, as Si–Si and Si–Si–Si (oxygen vacancies and divacancies) was made.

References

1. E.N. Ogawa, O. Aubel, Electrical breakdown in advanced interconnect dielectrics in *Advanced Interconnects for ULSI devices*. (Wiley, 2012).
2. A. Grill, *J. Vac. Sci. Technol. B* 34, 020801 (2016).
3. O.V. Pedreira, in *International Interconnect Technology Conference IITC2021* (Kyoto, Japan, 2021).
4. C. Adelmann, K. Sankaran, S. Dutta, A. Gupta, J.-P. Soulié, M. Siniscalchi, S. Kundu, M. Mao, V. Founta, N. Jourdan, in *ECS Meeting Abstracts* (2020), Vol. MA2020-01, pp. 1293.
5. L. Zhang, J.F. de Marneffe, N. Heylen, G. Murdoch, Z. Tokei, J. Boemmels, S. De Gendt, and M.R. Baklanov, *Appl. Phys. Lett.* 107, 092901 (2015).
6. J.M. Atkin, E. Cartier, T.M. Shaw, R.B. Laibowitz, and T.F. Heinz, *Appl. Phys. Lett.* 93, 122902 (2008).
7. J.M. Atkin, D. Song, T.M. Shaw, E. Cartier, R.B. Laibowitz, and T.F. Heinz, *J. Appl. Phys.* 103, 094104 (2008).
8. E.A. Smirnov, K. Vanstreels, P. Verdonck, I. Ciofi, D. Shamiryan, M.R. Baklanov, and M. Phillips, *Jap. J. Appl. Phys.* 50, 05EB03 (2011).
9. S. Shamuilia, V.V. Afanas'ev, P. Somers, A. Stesmans, Y.L. Li, Z. Tokei, G. Groeseneken, and K. Maex, *Appl. Phys. Lett.* 89, 2009 (2006).
10. A.A. Gismatulin, V.A. Gritsenko, D.S. Seregin, K.A. Vorotilov, and M.R. Baklanov, *Appl. Phys. Lett.* 115, 082904 (2019).
11. T.V. Perevalov, A.A. Gismatulin, A.E. Dolbak, V.A. Gritsenko, E.S. Trofimova, V.A. Pustovarov, D.S. Seregin, K.A. Vorotilov, and M.R. Baklanov, *Phys. Status Solidi A* 218, 2000654 (2021).
12. T.V. Perevalov, A.A. Gismatulin, D.S. Seregin, Y. Wang, H. Xu, V.N. Kruchinin, E.V. Spesivtsev, V.A. Gritsenko, K.A. Nasyrov, I.P. Prosvirin, J. Zhang, K.A. Vorotilov, and M.R. Baklanov, *J. Appl. Phys.* 127, 195105 (2020).
13. C. Wu, Y. Li, M.R. Baklanov, and K. Croes, *ECS J. Solid State Sci.* 4, N3065 (2015).
14. Y. Kayaba, and T. Kikkawa, *Jpn. J. Appl. Phys.* 47, 5314 (2008).
15. M.R. Baklanov, L. Zhao, E. Van Besien, and M. Pantouvaki, *Microelectron. Eng.* 88, 990 (2011).
16. E. Van Besien, M. Pantouvaki, L. Zhao, D. De Roest, M.R. Baklanov, Z. Tokei, and G. Beyer, *Microelectron. Eng.* 92, 59 (2012).
17. K. Vanstreels, I. Ciofi, Y. Barbarin, and M. Baklanov, *J. Vac. Sci. Technol. B* 31, 050604 (2013).

18. A.M. Urbanowicz, D. Shamiryan, A. Zaka, P. Verdonck, S. De Gendt, and M.R. Baklanov, *J. Electrochem. Soc.* 157, H565 (2010).
19. V. C. Ngwan, C. X. Zhu and A. Krishnamoorthy, in *2004 IEEE International Reliability Physics Symposium Proceedings*, 571 (2004).
20. T. Breuer, U. Kerst, C. Boit, E. Langer, H. Ruelke, and A. Fissel, *J. Appl. Phys.* 112, 124103 (2012).
21. V. Jousseaume, A. Zenasni, O. Gourhant, L. Favennec, and M.R. Baklanov, in *Advanced Interconnects for ULSI Technology*, edited by M. R. Baklanov, P. Ho, and E. Zschech (Wiley, 2012).
22. V.N. Kruchinin, V.A. Volodin, S.V. Rykhlitskii, V.A. Gritsenko, I.P. Posvirin, S. Xiaoping, and M.R. Baklanov, *Opt. Spectrosc.* 129, 681 (2021).
23. J. Frenkel, *Phys. Rev. B* 54, 647 (1938).
24. J. Frenkel, *Tech. Phys. USSR* 5, 685 (1938).
25. R.M. Hill, *Philos. Mag.* 23, 59 (1971).
26. H. Adachi, Y. Shibata, and S. Ono, *J. Phys. D: Appl. Phys.* 4, 988 (1971).
27. S.S. Makram-Ebeid, and M. Lannoo, *Phys. Rev. B* 25, 6406 (1982).
28. K.A. Nasyrov, and V.A. Gritsenko, *J. Appl. Phys.* 109, 093705 (2011).
29. L. Zhao, Z. Tokei, G. G. Gischia, H. Volders, and G. Beyer, in *Proceedings of International Interconnect Technology Conference* (IEEE, 2009), p. 206.
30. K.A. Nasyrov, V.A. Gritsenko, Y.N. Novikov, E.H. Lee, S.Y. Yoon, and C.W. Kim, *J. Appl. Phys.* 96, 4293 (2004).
31. V.A. Gritsenko, T.V. Perevalov, O.M. Orlov, and G.Y. Krasnikov, *Appl. Phys. Lett.* 109, 062904 (2016).
32. V.A. Pustovarov, V.S. Aliev, T.V. Perevalov, V.A. Gritsenko, and A.P. Eliseev, *J. Exp. Theor. Phys.* 111, 989 (2010).
33. V.A. Gritsenko, T.V. Perevalov, and D.R. Islamov, *Phys. Rep.* 613, 1 (2016).
34. T.V. Perevalov, D.V. Gulyaev, V.S. Aliev, K.S. Zhuravlev, V.A. Gritsenko, and A.P. Yelisseyev, *J. Appl. Phys.* 116, 244109 (2014).
35. V.A. Gritsenko, T.V. Perevalov, V.A. Voronkovskii, A.A. Gismatulin, V.N. Kruchinin, V.S. Aliev, V.A. Pustovarov, I.P. Prosvirin, Y. Roizin, and A.C.S. Appl, *Mater. Int.* 10, 3769 (2018).
36. L. Skuja, *J. Non-Crystalline Solids* 239, 16 (1998).
37. V.S. Kortov, A.F. Zatsepin, S.V. Gorbunov, and A.M. Murzakaev, *Phys. Solid State* 48, 1273 (2006).
38. K. Raghavachari, D. Ricci, and G. Pacchioni, *J. Chem. Phys.* 116, 825 (2002).
39. L.A. Bakaleinikov, M.V. Zamoryanskaya, E.V. Kolesnikova, V.I. Sokolov, and E.Y. Flegontova, *Phys. Solid. State.* 46, 1018 (2004).
40. Y. Ishikawa, A.V. Vasin, J. Salonen, S. Muto, V.S. Lysenko, A.N. Nazarov, N. Shibata, and V.P. Lehto, *J. Appl. Phys.* 104, 083522 (2008).